Electronic Journal of Biotechnology 65 (2023) 14–23

Contents lists available at ScienceDirect

Electronic Journal of Biotechnology

journal homepage: www.elsevier.com/locate/ejbt

Research Article

Therapeutic effect of biosynthesized silver nanoparticles on hypothyroidism induced in albino rats

Ebrahim Saied [a], Ahmed S. Hussein [b,*], Abdulaziz A. Al-Askar [c], Nadeem I. Elhussieny [d,e], Amr H. Hashem [a,*]

[a] Botany and Microbiology Department, Faculty of Science, Al-Azhar University, Nasr City 11884, Cairo, Egypt
[b] Zoology Department, Faculty of Science, Al-Azhar University, Cairo 11884, Egypt
[c] Department of Botany and Microbiology, Faculty of Science, King Saud University, P.O. Box 2455, Riyadh 11451, Saudi Arabia
[d] Department of Life Science and Chemistry, Constructor University, 28759 Bremen, Germany
[e] Institute of Environmental Biology and Biotechnology, University of Applied Sciences Bremen, Am Neustadtwall 30, 28199 Bremen, Germany

GRAPHICAL ABSTRACT

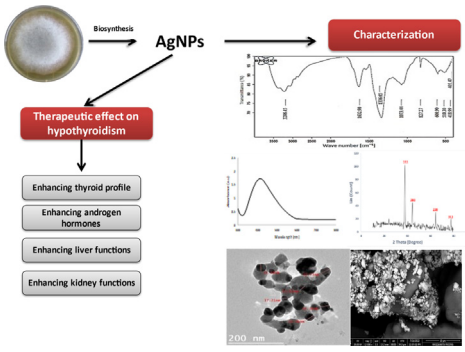

ARTICLE INFO

Article history:
Received 29 April 2023
Accepted 8 June 2023
Available online 10 July 2023

Keywords:
AgNPs
Biological synthesis
Hypothyroidism
Male albino rats
Nanoparticles
Potassium dichromate
Rhizopus oryzae
Silver nanoparticles
Therapeutic effect

ABSTRACT

Background: In this study, silver nanoparticles (AgNPs) were biosynthesized using *Rhizopus oryzae*. The therapeutic effect of AgNP treatment protocols for hypothyroidism induced in male albino rats via biochemical as well as hematological parameters, thyroid profile, and androgen male sex hormone (testosterone) was evaluated.

Results: FTIR, XRD, TEM, DLS, SEM, and EDX were used to comprehensively characterize the biosynthesized AgNPs. The AgNPs have a 17–35 nm diameter, according to the results of their characterization. The average size detected by XRD was 37.96 nm, while the average size of the biosynthesized AgNPs was 78 nm determined by DLS analysis. Furthermore, ALT, AST activity, urea, creatinine, and TSH levels revealed a significant increase in the untreated hypothyroidism group according to potassium dichromate-induced hypothyroidism compared to the normal control group. The untreated hypothyroidism group's FT3, FT4, and albumin levels, however, significantly decreased when compared to the normal control group. In contrast, when compared to the hypothyroidism-untreated group, the mean values of FT3, FT4, and TSH were all significantly higher and TSH was significantly lower in the hypothyroidism AgNPS-treated group. Furthermore, T. testosterone and F. testosterone levels revealed a significant decrease in untreated hypothyroidism group when compared to the normal control group. Contrarily, F. testosterone levels in the hypothyroidism-treated group were much higher than those in the hypothyroidism-untreated group.

Peer review under responsibility of Pontificia Universidad Católica de Valparaíso
* Corresponding authors.
E-mail addresses: ahmed_saber@azhar.edu.eg (A.S. Hussein), amr.hosny86@azhar.edu.eg (A.H. Hashem).

https://doi.org/10.1016/j.ejbt.2023.06.001

Conclusions: AgNPs were successfully biosynthesized which exhibited therapeutic potential to increase thyroid hormone levels and avoid the biochemical side effects of thyroid hormone deficiency in the animal model of hypothyroidism.

How to cite: Saied E, Hussein AS, Al-Askar AA, et al. Therapeutic effect of biosynthesized silver nanoparticles on hypothyroidism induced in albino rats. Electron J Biotechnol 2023;65. https://doi.org/10.1016/j.ejbt.2023.06.001.

1. Introduction

The thyroid gland is one of the important endocrine glands that play an essential and vital role in the metabolism and energy expenditure of the body [1]. This gland is responsible for the production, storage, and release of the thyroid hormones triiodothyronine (T3) and thyroxine (T4) [2]. All of the cells in the human body need them for appropriate development and differentiation [3]. The proper function of all metabolically active cells depends on the thyroid hormone. Disruption of the thyroid gland has the potential to have far-reaching consequences throughout the body [4]. Hypothyroidism, the second most common endocrine illness after diabetes, is characterized by thyroid gland under activity, resulting in thyroid hormone insufficiency [5]. Acquired hypothyroidism may develop from deficiencies in the processes that regulate thyroid hormone production [6]. Clinical evidence suggests a relationship between a low metabolic rate and the dysfunction of various body systems [7]. Multiple recent investigations have linked elevated ROS production to hypothyroidism [8].

Recently, there has been an unanticipated increase in the application of nanoparticles in a variety of fields, including molecular biology, physics, organic and inorganic chemistry, medicine, agriculture and material science [9,10,11,12,13,14,15,16]. Records show that the biological processes known as biosynthesis or "green synthesis" of nanoparticles are gradually replacing the physical and chemical techniques of producing metal and metal oxide nanoparticles [17,18,19]. In order to manufacture biocompatible metal or metal oxide nanoparticles in large quantities, the biological technique uses extracts from plants, bacteria, fungi, yeast, alga, and other microorganisms as reducing agents [20,21,22,23,24,25,26]. They are widely used since many fungal species have the ability to release enormous amounts of proteins or enzymes and because it is simple to trade them in laboratories [27]. Fungi have also gained more attention due to their tolerance and ability to bioaccumulate metals, since they are involved in the investigation of the biological creation of metallic nanomaterials [28,29]. As a result of their rapid growth rates and abundance of mass cells, many fungal species are also quite easy to maintain in a laboratory [30]. It has been demonstrated that the proteins and enzymes secreted by the aforementioned biological systems function as capping agents to give the nanoparticles stability and make them biocompatible for a variety of biological applications, as well as reducing agents to transform the bulk metal salts into the appropriate nanoparticles [31]. Due to their extensive antimicrobial potential, which includes antibacterial, antifungal, antiviral, and antiprotozoal capabilities, silver nanoparticles (AgNPs), a kind of metal nanoparticle, have been shown to have an immense variety of uses, notably in the field of biomedicine [32,33].

Treatments and therapies in medicine and healthcare have undergone a significant change as a result of the technical advance of regulating materials at the nanoscale. So, these properties allow the medicine to be properly targeted and distributed to tissues, limiting toxicity to organs and maximizing the drug's efficacy [34]. Nanoparticles are appealing for a variety of biological applications due to their high surface-to-volume ratio, ability to interact with molecular or cellular processes, and potential to influence their functioning [35]. Nanosystems' creative methodology has significantly improved illness detection, imaging, sensing, therapy, and management, thereby improving human health [36]. Silver nanoparticles (AgNPs) are one of the most attractive and popular metallic NP types, with uses in imaging, photography, biosensors, catalysis, and other fields [37,38]. Silver has been treasured since ancient times due to its ability to fight disease and its use in medical operations. Additionally, it has anti-inflammatory, anti-cancer, antiseptic, and antibacterial properties [39]. Innovative techniques have been used for the production of AgNPs in order to fully utilize the potential of silver in a variety of applications. The most common techniques of synthesis are chemical and physical, but since they require specialized equipment and harmful materials, they are expensive and dangerous [40]. AgNPs are one of the most valuable materials in the NPs with biomedical applications; they are widely employed in commercial goods, including cosmetics, nanomedical devices, apparel, sprays, home goods, and food items. Therefore, the study aimed to evaluate the therapeutic role of AgNP treatment protocol in order to protect adult male albino rats from developing potassium dichromate-induced hypothyroidism, which may be used as a promising therapy instead of traditional drugs because of its safety, low price and time consumption, in addition to discuss the safety profile as well as the pathophysiological changes related to the administration of AgNPs. Furthermore, the biosynthesized AgNPs were characterized by different techniques.

2. Materials and Methods

2.1. Materials

The analytical-grade chemicals used in this investigation, including sodium hydroxide (NaOH) and silver nitrate, an inorganic substance with the formula $AgNO_3$ and 99% purity, were acquired from Sigma-Aldrich in Egypt. In order to create AgNPs, $AgNO_3$ was used as a precursor. The purest cultured medium was all acquired from Merck in Germany (99% purity). In the current investigation, distilled water was used for all biological syntheses (dis. H_2O). Potassium dichromate was purchased from Sigma-Aldrich Chemical Company (Cairo, Egypt) in the form of a bottle containing 100 g of reddish powder, (Catalogue number 309176). Twenty-four adult male Wistar albino rats weighing about 100 ± 20 g were obtained from the animal house unit in the National Research Centre, Giza, Egypt. Throughout the experiment, the animals were kept in standard laboratory settings (12 h of light and 12 h of darkness) in a room with a constant temperature (24°C). Ad libitum tap water and typical commercial rat food were given to the rats. All researches were carried out in conformity with the Animal Ethical Committee of the National Research Center, Dokki, Giza, Egypt under the ethical number (Approval No. 18157).

2.2. Fungal growth conditions

Biosynthesis of AgNPs was carried out by *Rhizopus oryzae* which isolated and identified, deposited in Gene-bank with accession number MG518370 in our previous study [41]. *R. oryzae* was inoculated on malt extract agar (MEA) plates, then incubated for 3–5 d at 28°C ± 2°C then kept at 4°C for further use [42,43,44,45,46].

2.3. Biosynthesis of silver nanoparticles using the biomass filtrate of R. oryzae

Three disks (0.7 mm in diameter) of *R. oryzae* were grown on malt extract broth (MEB) medium, and the pH was adapted to 6.0, shaking conditions were used throughout the incubation of *R. oryzae* for 5 d at 28°C ± 2°C (150 rpm). Following the incubation period, deionized and sterile water were used to wash the collected biomass (15 g). After that, the cleaned biomass was reconstituted in 100 mL of distilled water at a temperature of 28°C ± 2°C and stirred for 3 d at 150 rpm. After that, the subsequently suspended biomass was centrifuged to get the fungal biomass filtrate, which was then utilized in the following procedure to create AgNPs. The pH was adjusted to pH 10, and 100 mL of fungal biomass filtrate was combined with 2.0 mM of silver nitrate (as a metal nanoparticle precursor) for 24 h in the dark at 28°C ± 2°C. After being extracted and dried for 24 h at 120°C, the filtrate developed a dark brown color [33,47].

2.4. Characterization of AgNPs

Different analytical methods were used to characterize the nanoparticles, including UV–Vis spectrophotometer (JENWAY 6305 spectrophotometer), Fourier transform infrared (FTIR) (Cary 660 FTIR model), Transmission Electron Microscopy [48] (JEM-1230, Japan, Akishima, Tokyo 196-8558), and Dynamic light scattering (DLS) was carried out using a Malvern Zetasizer Nanoseries compact scattering spectrometer from Malvern Instruments Ltd. in Worcestershire, UK, X-ray diffraction was obtained from Philips in Eindhoven, Netherlands, and SEM-EDX from JEOL in Tokyo, Japan. UV–Vis spectrophotometer absorbance measurements were taken between 300 and 800 nm. Fourier transform, infrared NP absorbance was recorded from 400 to 4000 cm^{-1}. The size of nanoparticles was analyzed using an X-Ray diffractometer at 40 KV and 30 mA at 37°C. Transmission electron microscopy was used to analyze the size and shape of the particles [49]. At 120 kV, TEM (Transmission Electron Microscopy) pictures were captured. Before the inspection, a carbon-coated TEM copper grid was sprayed with a colloidal solution of AgNPs and allowed to dry in the air. Dynamic light scattering (DLS) measurements were used to assess the AgNP particle size distribution. The polydispersity index (PDI), is the measure of homogeneity of the NPs solutions [29]. SEM with EDX analysis was used to evaluate the surface morphology and basic mapping of the produced AgNPs. The elemental composition of the sample was determined both qualitatively and quantitatively using an EDX device attached to the SEM.

2.5. Therapeutic effect of AgNP treatment protocols for hypothyroidism

2.5.1. Experimental design

Twenty-four adult male Wistar albino rats weighing about 100 ± 20 g were randomly assigned to different control and treatment groups. The experimental groups in common were divided into three groups (eight rats in each group) as follows: Group I: Rats from this group served as a normal control without any supplementation; Group II (Hypothyroidism-untreated group): Potassium dichromate was injected intraperitoneally into rats to cause hypothyroidism at a rate of 2 mg/kg/bw, which was subsequently dissolved in 1 mL of distilled water every day for two weeks before the rats were euthanized to confirm the condition [50]. Additionally, rats in Group III (Hypothyroidism AgNP-treated group) received a single intraperitoneal injection of AgNPs (0.75 mg/kg of body weight) for 30 d after receiving an i.p. injection of potassium dichromate to cause hypothyroidism [51]. Rats were allowed to acclimate for one week before the experiment began while standing for the whole four-week trial period during which drugs were administered. At the end of the experiment, blood samples were collected via retro-orbital under diethyl ether anesthesia. Each blood sample was divided into two parts; the first one was collected into a heparinized tube and used for the determination of hematological parameters; the second part was collected into non-heparinized tubes; after clotting, the samples were centrifuged at 4000 rpm for 15 min. Sera were further separated and used for further biochemical analysis.

2.5.2. Biochemical analyses

Liver enzymes were assessed. Serum levels of alanine transaminase [52] aspartate transaminase were determined, according to Reitman and Frankel [53]. Serum albumin concentration was determined according to the colorimetric method described by Doumas et al. [54]. The serum urea level was estimated according to the colorimetric method described by Fawcett and Scott [55]. The serum creatinine level was determined according to the colorimetric method described by Larsen [56]. Serum TSH, FT3, and FT4 levels were measured using immunoenzymatic tests (Roche Diagnostics-Mannheim, Germany). Estimation of serum testosterone level was adopted using the rat testosterone enzyme-linked immune-sorbent assay (ELISA) kit according to Tietz [57].

2.6. Statistical analysis

The data were shown as means (SE). A one-way ANOVA was used to finish the statistical analysis, and Dunnett's test was used to compare the treatment groups to the control group. Differences were considered significant at $p < 0.05$.

3. Results and Discussion

3.1. Biosynthesis and characterization of AgNPs

The potential of *R. oryzae* metabolites to biosynthesize AgNPs, which improve the production process, decrease aggregation, and produce a smaller size, was demonstrated in this work [58]. The color of the biomass filtrate changed when it was combined with metal precursors, which was the first indication that NPs were being biosynthesized. Santos et al. [59] synthesized the AgNPs from the extracellular extract of entomopathogenic fungi. Murillo-Rábago et al. [60] synthesized the AgNPs by using the supernatants of *Trichoderma harzianum* and *Ganoderma sessile*. Bukhari et al. [61], on the other hand, were successful in synthesizing AgNPs utilizing endophytic *Streptomyces laurentii*. Elsilk et al. [62] reported that the biofabrication of AgNPs occurred by using the biomass of *Streptomyces rochei* MS-37, a novel marine actinobacterium. Otherwise, some articles dealt with the biosynthesis of AgNPs via different biological extractions, such as plant extract or microbiological medium [63,64,65]. Also, Some et al. [66] synthesized AgNPs by utilizing leaf extract of *Morus indica L. V1*. Sudarsan et al. [67] biosynthesized AgNPs by using *Cytobacillus firmus* for photocatalytic and antimicrobial activities. In fact, the metallic nanoparticle is effective in several applications, especially in medical applications.

AgNPs are the most commercially successful NPs. Its toxicity has become a major issue due to its widespread usage in industrial,

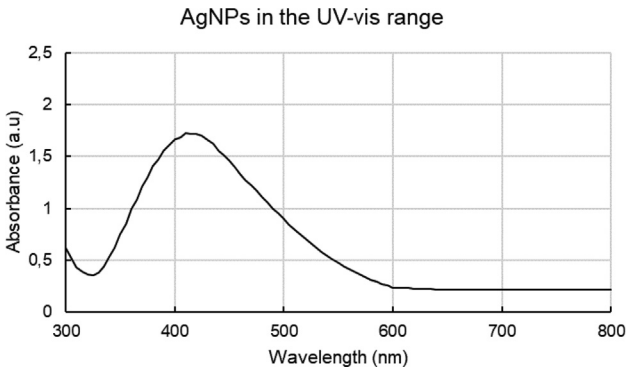

Fig. 1. Spectra of biosynthesized AgNPs in the UV-vis range at wavelengths of 300–800 nm.

biotechnological, and biomedical applications. In recent years, fascinating antibacterial and anticancer properties of biologically produced AgNPs have been revealed [68,69]. Due to the existence of proteins that reduce ions into particles, fungi can produce metallic nanoparticles. A physiochemical study and topographical inspections were used to characterize AgNPs. AgNPs' UV-visible spectra are displayed in Fig. 1. A color shift to deep brown in the UV-Vis spectrophotometer study for AgNP formation served as preliminary confirmation. Excitation of manufactured nanoparticles' surface plasmon resonance may be related to variations in color intensity [70]. The detection of a peak in the Ag NPs spectra at 410 nm provided evidence that AgNPs were produced by mycosynthesis [71]. Elshafei et al. [72], who identified a distinct peak of AgNPs at 410 nm, also came to the same conclusion. Khan et al. [73] synthesized AgNPs that exhibit a distinctive SPR band at 450 nm. According to Mujaddidi et al. [74], the plasmon absor-

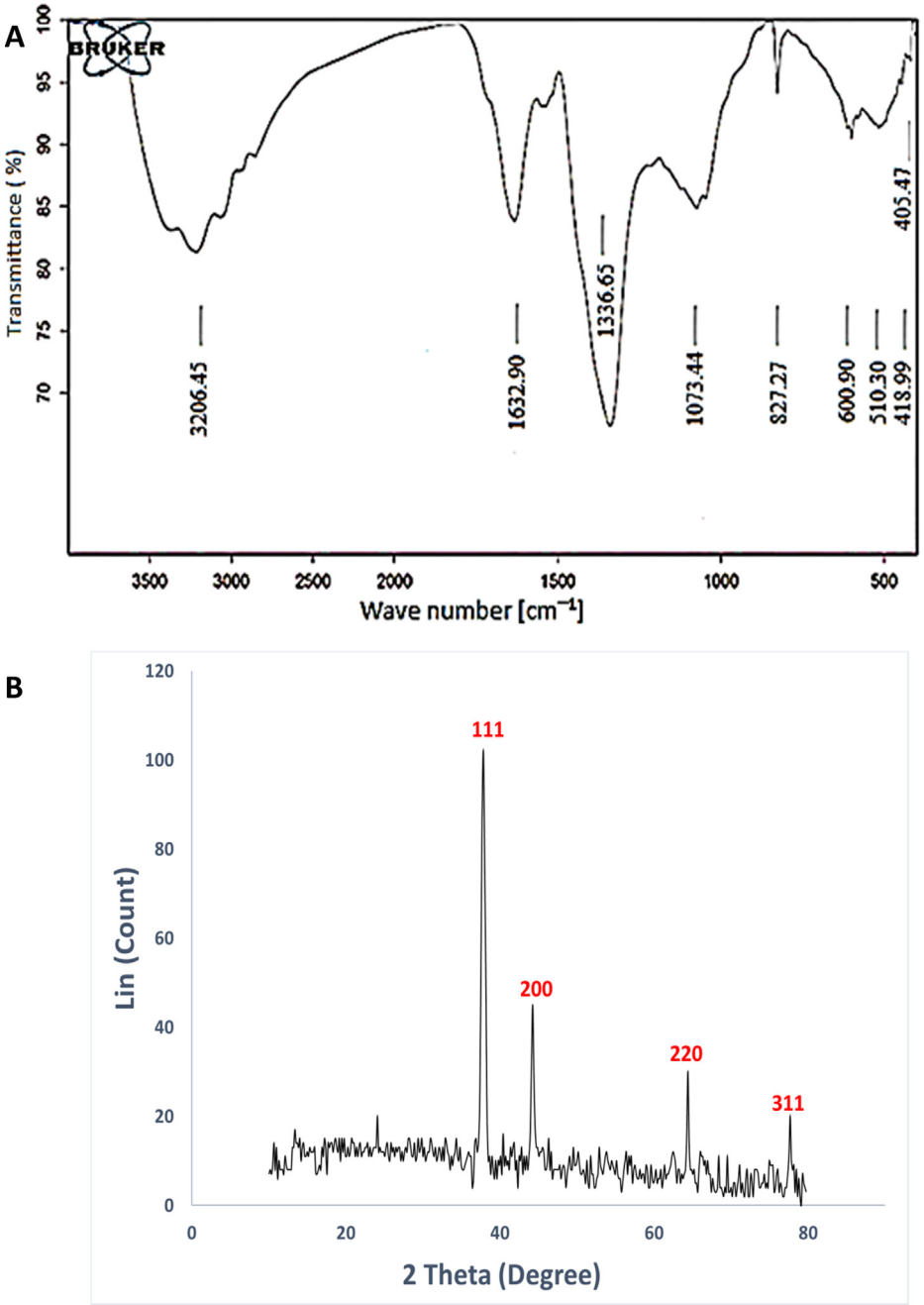

Fig. 2. (A) The FT-IR spectra of mycosynthesized AgNPs produced by *R. oryzae* metabolites; (B), XRD spectrum of biosynthesized AgNPs.

bance of AgNPs had a peak at 425 nm. On the other hand, smaller average AgNP sizes and larger concentrations of AgNPs are related to lower and higher maximum wavelength values, respectively [75]. According to Pallavi et al. [32], the produced AgNPs showed a prominent, distinctive absorption peak at 418 nm. Alharbi and Alsubhi [76] exhibit different bands at 429 and 435 nm, respectively, for AgNPs and AgNPs-cis.

Concerning FT-IR Analysis, proteins and enzymes found in the fungal biomass filtrate are crucial for the creation and stability of nanoparticles, according to the studies by Saravanan et al. [77]. The functional groups involved in the reduction and capping of the silver ions to the nanoscale are clarified in the country using FTIR analysis. As shown in Fig. 2A, FTIR analysis was used to investigate the interaction between AgNPs and *R. oryzae* supernatant. The biosynthesized AgNPs' FT-IR spectra revealed strong absorption peaks at 3206.45, 1632.90, 1336.65, 1073.44, 827.27, 600.90, 510.30, 418.99 and 405.47 cm^{-1}. The O-H stretching groups of phenols and alcohols or the N-H groups of amino acids in proteins are responsible for the peak at 3206 cm^{-1}, respectively [78,79]. The peak observed at 1632 cm^{-1} may correspond to the binding vibrations of the amide I band of proteins with N–H stretching [75]. The C-H bending form in alkanes is responsible for the shifted one at 1336 cm^{-1}. It is possible that the signal at 1073 cm^{-1} represented carboxylic (COO) residues [80]. An indication of the Amide IV (OCN) stretch bending for protein was a stretch at 827 and 600 cm^{-1}. The presence of a carbohydrate moiety may be the cause of the protein stretch band that was also seen at 510 cm^{-1} [81]. The calcinated AgNPs finally displayed a peak at 405 cm^{-1} [82]. Our findings show that proteins are present and that they attach to AgNPs, perhaps stabilizing them. These findings are in line with recent research that has shown that proteins play crucial roles in the production of AgNPs, serving as capping and stabilizing agents [32,74,76,83].

Fig. 2B shows the XRD pattern of the biosynthesized AgNPs, in which four distinct peaks were found at 2 θ degrees: 37.88°, 44.24°, 64.4°, and 77.68°. These peaks are indexed to the (1 1 1), (2 0 0), (2 2 0), and (3 1 1) crystal planes, respectively, demonstrating good alignment between the production of AgNPs and the crystalline phase of silver [29,32]. The face-centered cubic shape was seen in the peaks for various values of 2θ. Significant alignment to the studied facet (111) was indicated by the sharp peak at 2 = 37.8° (111), and the good purity of the prepared AgNPs. The average NP size was calculated using the Debye-Scherrer equation based on the XRD data. The FWHM (2θ) value for the AgNPs was 0.23111, and their average size was 37.96 nm. These outcomes are consistent with those reported in [65,72,84,85], where it was found that the range of the average particle size was between 5 and 20 nm. Sudarsan et al. [67] reported that the average size of the synthesized nanoparticles from endophytic bacteria was found to be 14.23 nm, which is consistent with our findings. According to Pallavi et al. [32], the average particle size of the AgNPs produced by *Streptomyces hirsutus* strain SNPGA-8 was 12.74 nm.

The morphological features and approximate sizes of NPs were investigated using TEM. In the TEM study (Fig. 3A), the produced nanomaterial was found to be spherical with a diameter of 17–35 nm. *Streptomyces hirsutus* strain SNPGA8 was successfully used by Pallavi et al. [32] to synthesize AgNPs with a TEM imaging range of 18–39 nm. According to research by Khan et al. [73], the produced nanomaterial has a spherical shape and a diameter between 4 and 12 nm, with an average size of around 8 nm. In the typical diameter range of 15–30 nm, Khan et al. [86] synthesized spheroidal-shaped PG-AgNPs. According to Kabir et al. [87], TEM was used to characterize the morphology of the *A. racemosus*-AgCl-NPs, which had an average diameter of about 17.0 nm. Khanal et al. [85] used TEM to analyze the size and morphology of AgNPs produced by *Rubus ellipticus* Sm, which is also noteworthy. They

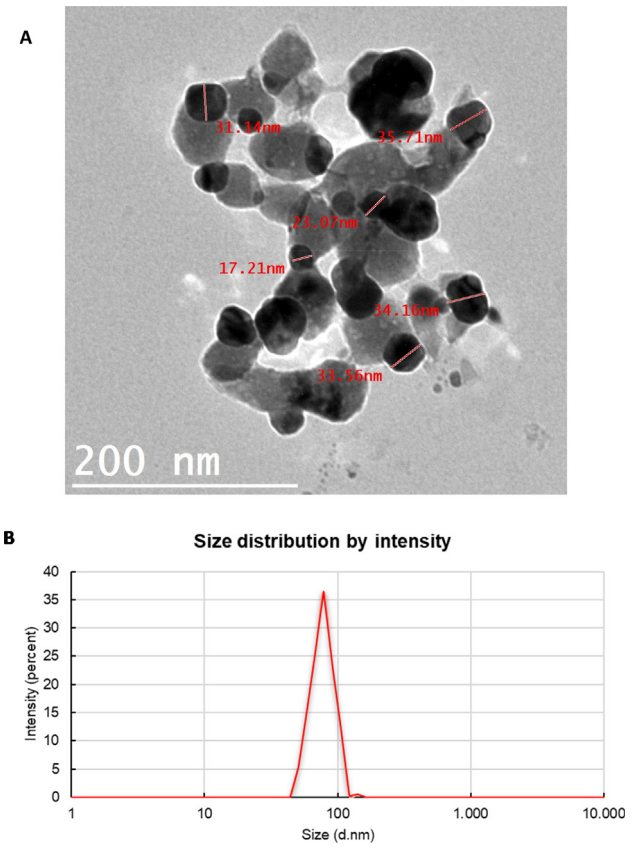

Fig. 3. (A) The spherical form of the biosynthesized AgNPs was visible in the TEM picture; (B) DLS analysis of biosynthesized AgNPs.

discovered the particles to be spherical, with sizes ranging from 13.85 to 34.30 nm. According to the TEM investigation [80], the chemicals found in *R. oryzae* FBF might be used to biosynthesize AgNPs with distinctive structures. Furthermore, the small size of the AgNPs created in this study has the potential to be used in a number of size-dependent biotechnological applications.

The size and size distribution of NPs in colloidal solutions were determined with the use of DLS analysis. The scattered intensities from time-dependent observations can be used to calculate the hydrodynamic diameter. The electrical layers on nanoparticle surfaces and the capping and stabilizing agents found in solution are frequently responsible for regulating the hydrodynamic diameter of these particles [88]. A small number of nanoparticles are needed for DLS in order to prevent numerous scattering effects. DLS is better suited to monitoring aggregation during the early phase since it is sensitive to the presence of aggregates. According to this study's DLS analysis, the average size of the biosynthesized AgNPs was 78 nm (36% intensity) (Fig. 3B). Khan et al. [86] state that the average size of the synthesized PG-AgNPs, as determined by the size distribution, is about 40 nm, with a PDI value of 0.321. Hashem et al. [80] demonstrated that the average size of the nanoparticles distribution histogram of biosynthesized AgNPs which ranged in size from 30 to 47 nm was 32.7 nm. Ag-NPs biofabricated using *Cytobacillus firmus* had an average hydrodynamic diameter of 55.8 nm, according to Saied et al. [25]. The homogeneity or heterogeneity of the colloidal NPs was assessed using the polydispersity index (PDI) value [29]. High homogeneity is indicated by a PDI value less than 0.4, whereas low homogeneity is indicated by a value greater than 0.4, and a heterogeneous solution is indicated by a value greater than 1. We discovered a PDI value of 0.031 throughout our study.

SEM was used to examine the morphology of biosynthesized AgNPs. The SEM examination of biosynthesized AgNPs is shown in Figs. 4A-B. This study confirmed the spherical shape and small size of the nanoparticles found in the XRD analysis. The scanning electron microscopy also showed that the powder particles have a slightly aggregated structure. A small number of AgNPs were seen clustering together to produce bigger particles. This outcome was in line with the AgNPs found in earlier researches [74,89]. Due to their high electrical conductivity, metal nanoparticles like silver and gold can be easily scanned with a SEM. SEM is unable to view the internal structure of materials, although it can offer insightful data on particle integrity and aggregation [89]. The Ag element was present, according to the AgNPs' EDX profile. The Ag element is present at 62.7% weight percentage, as shown by the EDX profile (Fig. 4B). O and Ag contribute 37.2% and 62.7% of the total weight, respectively. O has the greatest atomic percentage (80%), followed by Ag with 19%.

3.2. In vivo therapeutic effect of AgNPS on induced hypothyroidism in adult male albino rats.

One of the most prevalent endocrine conditions, hypothyroidism, is mostly a result of thyroid gland problems that induce a decrease in thyroid hormone production and secretion [90]. Due to its widespread use as a heavy metal in numerous industries, potassium dichromate was selected for this study's hypothyroidism experiment [91]. Therefore, we sought to evaluate the protective effect of AgNPs on potassium dichromate-induced hypothyroidism in male albino rats. In addition, male albino rodents were recruited for this study because males are more susceptible to occupational infertility exposure and because female hormones may interfere. However, females have a higher incidence of hypothyroidism [92]. In the present study, the mean values of TSH, Ft3, Ft4, T. testosterone and F. testosterone levels revealed a high and significant difference in comparison between all groups

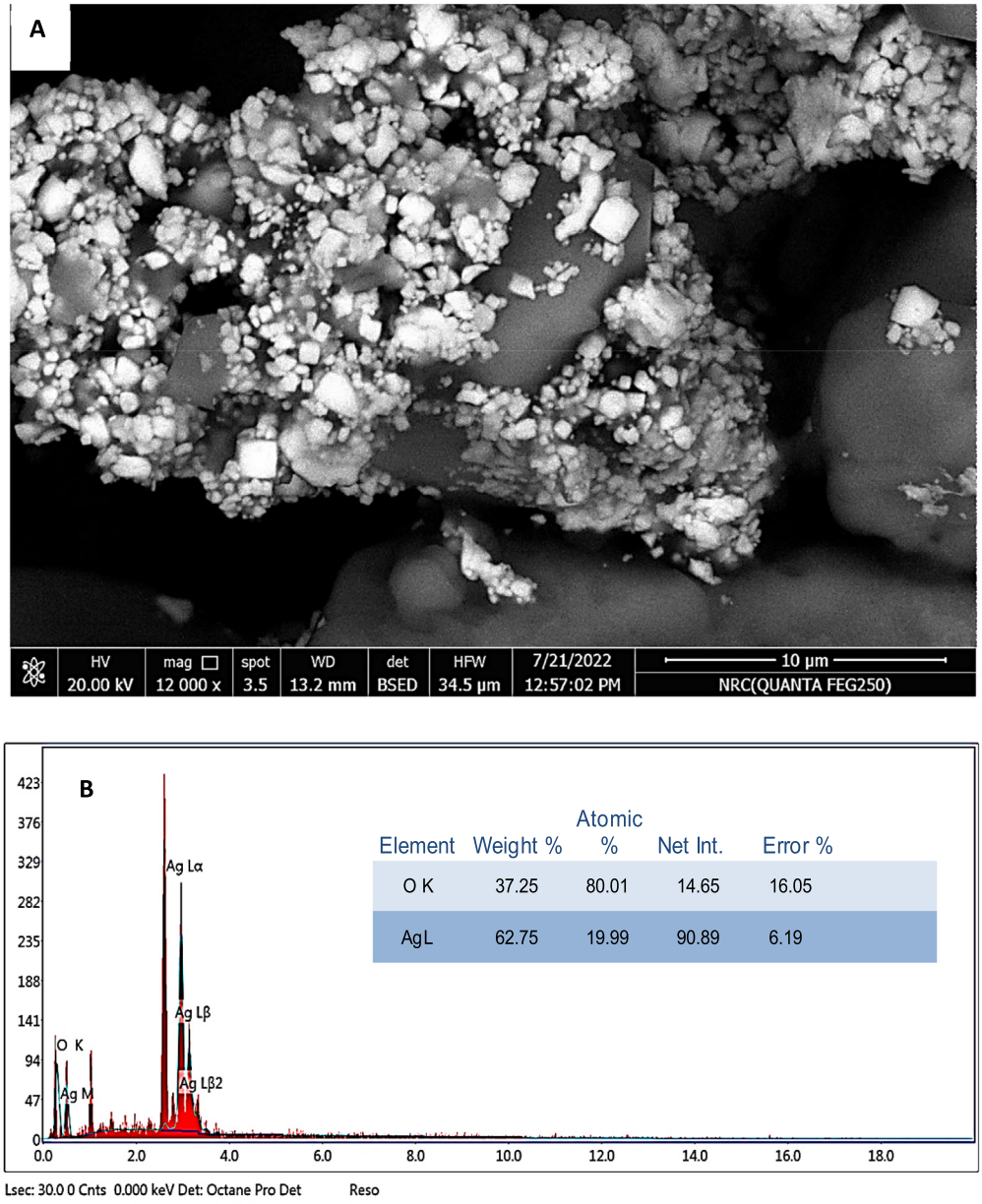

Fig. 4. (A) SEM image of AgNPs; (B) EDX spectrum of the formed AgNPs.

Table 1
Effect of AgNPs on thyroid profile and androgen hormones in rats subjected to Hypothyrodism..

Experimental groups	Thyroid profile			Androgen Hormones	
	TSH (UIu/mL)	Ft3 (ng/dl)	Ft4 (ng/dl)	Total Testosterone (Pg/mL)	Free Testosterone (Pg/mL)
Group I: (Normal)	4.2 ± 0.4^{c}	1.5 ± 0.1^{a}	1.3 ± 0.1^{b}	7.3 ± 0.4^{a}	3.6 ± 0.3^{a}
Group II: (Hypothyroidism)	7.2 ± 0.5^{a}	0.4 ± 0.0^{b}	2.0 ± 0.2^{a}	1.5 ± 0.1^{c}	0.7 ± 0.1^{c}
Group III: (Hypothyroidism + AgNPs)	5.3 ± 0.4^{b}	0.4 ± 0.1^{b}	1.3 ± 0.1^{b}	2.1 ± 0.2^{b}	2.9 ± 0.2^{b}

Mean value represents mean of 8 records ± SE. Means with dissimilar superscript letter are significantly different at $P < 0.05$.

of the animal model, including positive treated and untreated groups, as illustrated in Table 1.

According to potassium dichromate-induced hypothyroidism (group II), the blood TSH levels of the untreated hypothyroidism group increase dramatically when compared to the normal control group's mean values. Nonetheless, Ft3 and Ft4 levels were significantly lower in the untreated hypothyroidism group than in the normal control group. Hassanin et al. [93] reported similar findings, attributing the decrease in thyroid hormone production by follicular cells to increased OS and ROS created by the conversion of potassium dichromate to its trivalent form. However, Mahmood et al. [94] reported that the decrease in T3 and T4 was due to an active combination of chromium and globulins. This, in turn, hampered thyroglobulin proteolysis. In comparison to the untreated group (group II), the mean values of T3 and T4 were significantly higher and the mean value of TSH was significantly lower in the hypothyroidism AgNPs-treated group (group III) due to the capacity of metal nanoparticles to directly target the damaged organ, thereby decreasing unwanted effects, a better improvement in thyroid function with AgNPs was predicted. In accordance with Kalishwaralal et al. [95], it has distinct physical and chemical properties and is used in a variety of applications, such as antibacterial and drug delivery systems.

The results of serum T. and F. testosterone levels revealed a highly significant decrease in the untreated hypothyroidism group when compared to the mean values in the normal control group. However, there are no significant differences in serum T. testosterone levels between the hypothyroidism-treated group and the untreated group as compared to the mean values in the untreated group. On the other hand, the F. testosterone level in the hypothyroidism-treated group was significantly elevated as compared to the hypothyroidism-untreated group.

Liver and kidney function tests, including serum (ALT, AST, Albumin, Urea, Creatinine and Uric acid), are illustrated in Table 2. According to the one-way ANOVA test, the represented data of ALT and AST activity as well as albumin level showed highly significant differences at (P<0.001) in comparison between all groups of the animal model, including treated and untreated groups. The results of ALT activity showed a significant increase in positive control group (GII) induced hypothyroidism by potassium dichromate when compared to the mean values in normal rats (GI: Negative control). Nevertheless, ALT activity in the positive treated group (GIII: Hypothyroidism-treated group) Rats induced Hypothyroidism by potassium dichromate followed by administration of silver oxide nanoparticles (AgNPs) showed a highly significant decrease when compared to the mean values in the positive control (GII: Hypothyroidism-untreated group). Moreover, AST activity showed a significant increase in the positive untreated group when compared to the mean values in the negative control. While AST activity showed a significant decrease in positive treated group as compared to the mean values in Positive untreated group. However, serum albumin levels indicated a significant decrease in positive untreated group when compared to the mean values in the negative control. Though albumin levels were significantly increased in the positive treated group as compared to the positive untreated group.

The results of serum urea levels in the positive control group revealed a highly significant increase ($P < 0.001$) as compared to the mean corresponding values in the negative control. However, urea levels showed a significant decrease ($P < 0.01$) in the positive treated group as compared to the mean values in the positive untreated group. Furthermore, serum creatinine levels in the positive control group revealed a significant increase ($P < 0.05$) in the positive control group when compared to the mean corresponding values in the negative control. However, creatinine levels showed no significant differences in positive treated group when compared to the mean values in the positive untreated group. On the other hand, there are no significant differences in Uric acid level in comparison between all experimental groups of animals.

4. Conclusions

R. oryzae was used in the current study to biosynthesize AgNPs through ecofriendly method. Results indicated that biosynthesized AgNPs whose diameter ranged from 17 to 35 nm and were spherical in shape. Besides, biosynthesized AgNPs have the therapeutic potential to raise thyroid hormone levels and attenuate its complications, which can be further evaluated by thyroid hormone deficiency in animal model-induced hypothyroidism. We believe that nanomaterials would dramatically promote the development of medicine, and silver nanoparticles are expected to have more exciting influences in these fields.

Author contributions

- Study conception and design: E Saied, AS Hussein, AH Hashem.
- Methodology: E Saied, AS Hussein, AH Hashem.
- Data collection: AA Al-Askar, NI Elhussieny.
- Analysis and interpretation of results: E Saied, AS Hussein, AA Al-Askar, NI Elhussieny, AH Hashem.

Table 2
Effect of AgNPs on liver and kidney functions in rats subjected to Hypothyrodism.

Experimental groups	Liver Function Tests			Kidney Function Tests		
	ALT (IU/mL)	AST (IU/mL)	Albumin (g/dl)	Urea (mg/dl)	Creatinine (mg/dl)	Uric Acid (mg/dl)
Group I: (Normal)	48.4 ± 3.3^{b}	19.5 ± 1.4^{c}	4.2 ± 0.1^{a}	45.5 ± 2.1^{c}	0.5 ± 0.0^{c}	4.4 ± 0.4^{b}
Group II: (Hypothyroidism)	104.3 ± 3.3^{a}	110.4 ± 6.1^{a}	3.0 ± 0.2^{c}	66.8 ± 4.3^{a}	1.0 ± 0.2^{a}	5.1 ± 0.7^{a}
Group III: (Hypothyroidism + AgNPs)	49.9 ± 1.9^{b}	57.8 ± 7.3^{b}	3.8 ± 0.2^{b}	51.5 ± 4.1^{b}	0.7 ± 0.1^{b}	4.1 ± 0.5^{c}

Mean value represents mean of 8 records ± SE. Means with dissimilar superscript letter are significantly different at $P < 0.05$.

- Draft manuscript preparation: E Saied, AS Hussein, AH Hashem.
- Revision of the results and approved the final version of the manuscript: E Saied, AS Hussein, AA Al-Askar, NI Elhussieny, AH Hashem.

Financial support

The authors extend their appreciation to the researcher supporting project number (RSP2023R505), King Saud University, Riyadh, Saudi Arabia for funding this work.

Conflict of interest

There are no conflicts to declare.

Acknowledgments

The authors express their sincere thanks to the Faculty of Science (Boys), Al-Azhar University, Cairo, Egypt for providing the necessary research facilities. Also, the authors extend their appreciation to the researcher supporting project number (RSP2023R505), King Saud University, Riyadh, Saudi Arabia for funding this work.

Data availability

The data made available upon requested.

References

[1] Tortora GJ, Derrickson B. The cardiovascular system: blood vessels and hemodynamics. Principles Anatomy Physiol 2012:610–35.
[2] De Felice M, Postiglione MP, Di Lauro R. Minireview: Thyrotropin receptor signaling in development and differentiation of the thyroid gland: Insights from mouse models and human diseases. Endocrinology 2004;145(9):4062–7. https://doi.org/10.1210/en.2004-0501. PMid: 15231702.
[3] Jayaprakasha GK, Jagan Mohan Rao L, Sakariah KK. Antioxidant activities of curcumin, demethoxycurcumin and bisdemethoxycurcumin. Food Chem 2006;98(4):720–4. https://doi.org/10.1016/j.foodchem.2005.06.037.
[4] Patil VV, Dhurvey VT. Exposure to sodium fluoride affects thyroid follicular cells in albino rats. Int J Plant, Animal Environ Sci 2015;5(1):56–61.
[5] Ayuob NN, El-Shitany NA, Alama MN. Thymoquinone protects against hypothyroidism-induced cardiac histopathological changes in rats through a nitric oxide/antioxidant mechanism. Biomed Res 2016;27(1):93–102.
[6] Hayat HN, Tahir TM, Munir MB, et al. Effect of methimazole-induced hypothyroidism on histological characteristics of parotid gland of albino rat. J Ayub Med Coll Abbottabad 2010;22(3):22–7. PMid: 22338410.
[7] Golden SH, Robinson KA, Saldanha I, et al. Prevalence and incidence of endocrine and metabolic disorders in the United States: A comprehensive review. J Clin Endocrinol Metab 2009;94(6):1853–78. https://doi.org/10.1210/jc.2008-2291. PMid: 19494161.
[8] Nanda N. Oxidative stress in hypothyroidism. Int J Clin Exp Physiol 2016;3(1):4–9.
[9] Hashem AH, Shehabeldine AM, Ali OM, et al. Synthesis of chitosan-based gold nanoparticles: antimicrobial and wound-healing activities. Polymers 2022;14(11):2293. https://doi.org/10.3390/polym14112293. PMid: 35683965.
[10] Doghish AS, Hashem AH, Shehabeldine AM, et al. Nanocomposite based on gold nanoparticles and carboxymethyl cellulose: Synthesis, characterization, antimicrobial, and anticancer activities. J Drug Delivery Sci Technol 2022;77:103874. https://doi.org/10.1016/j.jddst.2022.103874.
[11] Hashem AH, Hasanin M, Kamel S, et al. A new approach for antimicrobial and antiviral activities of biocompatible nanocomposite based on cellulose, amino acid and graphene oxide. Colloids Surf B Biointerfaces 2022;209(Part 1):112172. https://doi.org/10.1016/j.colsurfb.2021.112172. PMid: 34715596.
[12] Hashem AH, Saied E, Ali OM, et al. Pomegranate peel extract stabilized selenium nanoparticles synthesis: Promising antimicrobial potential, antioxidant activity, biocompatibility, and hemocompatibility. Appl Biochem Biotechnol 2023. https://doi.org/10.1007/s12010-023-04326-y. PMid: 36705842.
[13] Hashem AH, El-Sayyad GS. Antimicrobial and anticancer activities of biosynthesized bimetallic silver-zinc oxide nanoparticles (Ag-ZnO NPs) using pomegranate peel extract. Biomass Convers Biorefin 2023. https://doi.org/10.1007/s13399-023-04126-8.
[14] Hashem AH, Al-Askar AA, Haponiuk J, et al. Biosynthesis, characterization, and antifungal activity of novel trimetallic copper oxide-selenium-zinc oxide nanoparticles against some mucorales fungi. Microorganisms 2023;11(6):1380. https://doi.org/10.3390/microorganisms11061380.
[15] Hashem AH, Al Abboud MA, Alawlaqi MM, et al. Synthesis of nanocapsules based on biosynthesized nickel nanoparticles and potato starch: Antimicrobial, antioxidant, and anticancer activity. Starch-Stärke 2022;74(1–2):2100165. https://doi.org/10.1002/star.202100165.
[16] Salem SS, Hashem AH, Sallam A-A-M, et al. Synthesis of silver nanocomposite based on carboxymethyl cellulose: Antibacterial, antifungal and anticancer activities. Polymers 2022;14(16):3352. https://doi.org/10.3390/polym14163352. PMid: 36015608.
[17] Marouzi S, Sabouri Z, Darroudi M. Greener synthesis and medical applications of metal oxide nanoparticles. Ceram Int 2021;47(14):19632–50. https://doi.org/10.1016/j.ceramint.2021.03.301.
[18] Saied E, Mekky AE, Al-Askar AA, et al. *Aspergillus terreus*-mediated selenium nanoparticles and their antimicrobial and photocatalytic activities. Crystals 2023;13(3):450. https://doi.org/10.3390/cryst13030450.
[19] lashin I, Hasanin M, Hassan SAM, et al. Green biosynthesis of zinc and selenium oxide nanoparticles using callus extract of *Ziziphus spina-christi*: characterization, antimicrobial, and antioxidant activity. Biomass Convers Biorefin 2023;13:10133–46. https://doi.org/10.1007/s13399-021-01873-4.
[20] Abd Elkodous M, El-Husseiny HM, El-Sayyad GS, et al. Recent advances in waste-recycled nanomaterials for biomedical applications: Waste-to-wealth. Nanotechnol Rev 2021;10(1):1662–739. https://doi.org/10.1515/ntrev-2021-0099.
[21] Albalawi MA, Abdelaziz AM, Attia MS, et al. Mycosynthesis of silica nanoparticles using *Aspergillus niger*: control of *Alternaria solani* causing early blight disease, induction of innate immunity and reducing of oxidative stress in eggplant. Antioxidants 2022;11(12):2323. https://doi.org/10.3390/antiox11122323. PMid: 36552531.
[22] Ali OM, Hasanin MS, Suleiman WB, et al. Green biosynthesis of titanium dioxide quantum dots using watermelon peel waste: Antimicrobial, antioxidant, and anticancer activities. Biomass Convers Biorefin 2022. https://doi.org/10.1007/s13399-022-02772-y.
[23] El-Naggar ME, Hasanin M, Hashem AH. Eco-friendly synthesis of superhydrophobic antimicrobial film based on cellulose acetate/polycaprolactone loaded with the green biosynthesized copper nanoparticles for food packaging application. J Polym Environ 2022;30:1820–32. https://doi.org/10.1007/s10924-021-02318-9.
[24] Hashem AH, Selim TA, Alruhaili MH, et al. Unveiling antimicrobial and insecticidal activities of biosynthesized selenium nanoparticles using prickly pear peel waste. J Funct Biomater 2022;13(3):112. https://doi.org/10.3390/jfb13030112. PMid: 35997450.
[25] Saied E, Hashem AH, Ali OM, et al. Photocatalytic and antimicrobial activities of biosynthesized silver nanoparticles using *Cytobacillus firmus*. Life 2022;12(9):1331. https://doi.org/10.3390/life12091331. PMid: 36143368.
[26] Saravanan M, Barabadi H, Vahidi H. Green nanotechnology: isolation of bioactive molecules and modified approach of biosynthesis. In: Patra C, Ahmad I, Ayaz M, editors. Biogenic nanoparticles for cancer theranostics. Elsevier; 2021. p. 101–22. , https://doi.org/10.1016/B978-0-12-821467-1.00005-7.
[27] Salem SS, Fouda A. Green synthesis of metallic nanoparticles and their prospective biotechnological applications: an overview. Biol Trace Elem Res 2021;199:344–70. https://doi.org/10.1007/s12011-020-02138-3. PMid: 32377944.
[28] Mittal S, Roy A. Fungus and plant-mediated synthesis of metallic nanoparticles and their application in degradation of dyes. In: Shah M, Dave S, Das J, editors. Photocatalytic degradation of dyes. Elsevier; 2021. p. 287–308. , https://doi.org/10.1016/B978-0-12-823876-9.00009-3.
[29] Soliman AM, Abdel-Latif W, Shehata IH, et al. Green approach to overcome the resistance pattern of *Candida* spp. using biosynthesized silver nanoparticles fabricated by *Penicillium chrysogenum* F9. Biol Trace Elem Res 2021;199:800–11. https://doi.org/10.1007/s12011-020-02188-7. PMid: 32451695.
[30] Shaheen TI, Salem S, Fouda A. Current advances in fungal nanobiotechnology: mycofabrication and applications. In: Lateef A, Gueguim-Kana EB, Dasgupta N, editors. Microbial nanobiotechnology. materials horizons: from nature to nanomaterials. Singapore: Springer; 2021. p. 113–43. , https://doi.org/10.1007/978-981-33-4777-9_4.
[31] Rai M, Ingle AP, Trzcińska-Wencel J, et al. Biogenic silver nanoparticles: what we know and what do we need to know? Nanomaterials 2021;11(11):2901. https://doi.org/10.3390/nano11112901. PMid: 34835665.
[32] Pallavi S, Rudayni HA, Bepari A, et al. Green synthesis of Silver nanoparticles using *Streptomyces hirsutus* strain SNPGA-8 and their characterization, antimicrobial activity, and anticancer activity against human lung carcinoma cell line A549. Saudi J Biol Sci 2022;29(1):228–38. https://doi.org/10.1016/j.sjbs.2021.08.084. PMid: 35002413.
[33] Saqib S, Faryad S, Afridi MI, et al. Bimetallic assembled silver nanoparticles impregnated in *Aspergillus fumigatus* extract damage the bacterial membrane surface and release cellular contents. Coatings 2022;12(10):1505. https://doi.org/10.3390/coatings12101505.
[34] Li S, Tan L, Meng X. Nanoscale metal-organic frameworks: synthesis, biocompatibility, imaging applications, and thermal and dynamic therapy of tumors. Adv Funct Mater 2020;30(13):1908924. https://doi.org/10.1002/adfm.201908924.

[35] Abd Elkodous M, El-Sayyad GS, Abdelrahman IY, et al. Therapeutic and diagnostic potential of nanomaterials for enhanced biomedical applications. Colloids Surf B Biointerfaces 2019;180:411–28. https://doi.org/10.1016/j.colsurfb.2019.05.008. PMid: 31085460.
[36] Singh R, Sharma A, Saji J, et al. Smart nanomaterials for cancer diagnosis and treatment. Nano Convergence 2022;9(1):21. https://doi.org/10.1186/s40580-022-00313-x. PMid: 35569081.
[37] Lee SH, Jun B-H. Silver nanoparticles: Synthesis and application for nanomedicine. Int J Mol Sci 2019;20(4):865. https://doi.org/10.3390/ijms20040865. PMid: 30781560.
[38] Li Y, Liao Q, Hou W, et al. Silver-based surface plasmon sensors: Fabrication and applications. Int J Mol Sci 2023;24(4):4142. https://doi.org/10.3390/ijms24044142. PMid: 36835553.
[39] Verma P, Maheshwari SK. Applications of silver nanoparticles in diverse sectors. Int J Nano Dimens 2019;10(1):18–36.
[40] Habeeb Rahuman HB, Dhandapani R, Narayanan S, et al. Medicinal plants mediated the green synthesis of silver nanoparticles and their biomedical applications. IET Nanobiotechnol 2022;16(4):115–44. https://doi.org/10.1049/nbt2.12078. PMid: 35426251.
[41] Suleiman W, El-Skeikh H, Abu-Elreesh G, et al. Isolation and screening of promising oleaginous Rhizopus sp and designing of Taguchi method for increasing lipid production. J Innov Pharm Biol Sci 2018;5(1):8–15.
[42] Fouda A, Khalil A, El-Sheikh H, et al. Biodegradation and detoxification of bisphenol-A by filamentous fungi screened from nature. J Adv Biol Biotechnol 2015;2(2):123–32. https://doi.org/10.9734/JABB/2015/13959.
[43] Hashem AH, Hasanin MS, Khalil AMA, et al. Eco-green conversion of watermelon peels to single cell oils using a unique oleaginous fungus: *Lichtheimia corymbifera* AH13. Waste Biomass Valoriz 2020;11:5721–32. https://doi.org/10.1007/s12649-019-00850-3.
[44] Suleiman W, El-Sheikh H, Abu-Elreesh G, et al. Recruitment of *Cunninghamella echinulata* as an Egyptian isolate to produce unsaturated fatty acids. Res J Pharm, Biol Chem Sci 2018;9(1):764–74.
[45] Khalil AMA, Hashem AH. Morphological changes of conidiogenesis in two *Aspergillus* species. J Pure Appl Microbiol 2018;12(4):2041–8. https://doi.org/10.22207/JPAM.12.4.40.
[46] Hasanin MS, Hashem AH. Eco-friendly, economic fungal universal medium from watermelon peel waste. J Microbiol Methods 2020;168:105802. https://doi.org/10.1016/j.mimet.2019.105802. PMid: 31809830.
[47] Chandankere R, Chelliah J, Subban K, et al. Biotechnology: Pleiotropic functions and biological potentials of silver nanoparticles synthesized by an endophytic fungus. Front Bioeng Biotechnol 2020;8:95. https://doi.org/10.3389/fbioe.2020.00095. PMid: 32154230.
[48] Malekkiani M, Heshmati Jannat Magham A, Ravari F, et al. Facile fabrication of ternary MWCNTs/ZnO/Chitosan nanocomposite for enhanced photocatalytic degradation of methylene blue and antibacterial activity. Sci Rep 2022;12(1):5927. https://doi.org/10.1038/s41598-022-09571-5. PMid: 35396520.
[49] Jain AK, Thareja S. *In vitro* and *in vivo* characterization of pharmaceutical nanocarriers used for drug delivery. Artif Cells Nanomed Biotechnol 2019;47(1):524–39. https://doi.org/10.1080/21691401.2018.1561457. PMid: 30784319.
[50] ElBakry RH, Tawfik SM. Histological study of the effect of potassium dichromate on the thyroid follicular cells of adult male albino rat and the possible protective role of ascorbic acid (vitamin C). J Microsc Ultrastruct 2014;2(3):137–50.
[51] Sarhan OMM, Hussein RM. Effects of intraperitoneally injected silver nanoparticles on histological structures and blood parameters in the albino rat. Int J Nanomed 2014;9(1):1505–17. https://doi.org/10.2147/IJN.S56729. PMid: 24711700.
[52] Salama B, Alzahrani KJ, Alghamdi KS, et al. Silver nanoparticles enhance oxidative stress, inflammation, and apoptosis in liver and kidney tissues: Potential protective role of thymoquinone. Biol Trace Element Res 2023;201:2942–54. https://doi.org/10.1007/s12011-022-03399-w. PMid: 36018545.
[53] Reitman S, Frankel S. A colorimetric method for the determination of serum glutamic oxalacetic and glutamic pyruvic transaminases. Am J Clin Pathol 1957;28(1):56–63. https://doi.org/10.1093/ajcp/28.1.56. PMid: 13458125.
[54] Doumas BT, Watson WA, Biggs HG. Albumin standards and the measurement of serum albumin with bromcresol green. Clin Chim Acta 1971;31(1):87–96. https://doi.org/10.1016/0009-8981(71)90365-2. PMid: 5544065.
[55] Fawcett J, Scott J. A rapid and precise method for the determination of urea. J Clin Pathol 1960;13(2):156–9. https://doi.org/10.1136/jcp.13.2.156. PMid: 13821779.
[56] Larsen K. Creatinine assay by a reaction-kinetic principle. Clin Chim Acta 1972;41:209–17. https://doi.org/10.1016/0009-8981(72)90513-x. PMid: 4645233.
[57] Tietz NW. Clinical guide to laboratory tests. Clinical Guide to Laboratory Tests 1995:1096.
[58] Loshchinina EA, Vetchinkina EP, Kupryashina MA. Diversity of biogenic nanoparticles obtained by the fungi-mediated synthesis: A review. Biomimetics 2022;8(1):1. https://doi.org/10.3390/biomimetics8010001. PMid: 36648787.
[59] Santos TS, dos Passos EM, Seabra MGJ, et al. Entomopathogenic fungi biomass production and extracellular biosynthesis of silver nanoparticles for bioinsecticide action. Appl Sci 2021;11(6):2465. https://doi.org/10.3390/app11062465.
[60] Murillo-Rábago EI, Vilchis-Nestor AR, Juarez-Moreno K, et al. Optimized synthesis of small and stable silver nanoparticles using intracellular and extracellular components of fungi: An alternative for bacterial inhibition. Antibiotics 2022;11(6):800. https://doi.org/10.3390/antibiotics11060800. PMid: 35740206.
[61] Bukhari SI, Hamed MM, Al-Agamy MH, et al. Biosynthesis of copper oxide nanoparticles using *Streptomyces* MHM38 and its biological applications. J Nanomater 2021;2021:6693302. https://doi.org/10.1155/2021/6693302.
[62] Elsilk SE, Khalil MA, Aboshady TA, et al. *Streptomyces rochei* MS-37 as a novel marine actinobacterium for green biosynthesis of silver nanoparticles and their biomedical applications. Molecules 2022;27(21):7296. https://doi.org/10.3390/molecules27217296. PMid: 36364123.
[63] Baran A, Keskin C, Baran MF, et al. Ecofriendly synthesis of silver nanoparticles using *Ananas comosus* fruit peels: Anticancer and antimicrobial activities. Bioinorg Chem Appl 2021;2021:2058149. https://doi.org/10.1155/2021/2058149. PMid: 34887909.
[64] Chugh D, Viswamalya V, Das B. Green synthesis of silver nanoparticles with algae and the importance of capping agents in the process. J Genet Eng Biotechnol 2021;19(1):126. https://doi.org/10.1186/s43141-021-00228-w. PMid: 34427807.
[65] Ghoshal G, Singh M. Characterization of silver nano-particles synthesized using fenugreek leave extract and its antibacterial activity. Mater Sci Energy Technol 2022;5:22–9. https://doi.org/10.1016/j.mset.2021.10.001.
[66] Some S, Bulut O, Biswas K, et al. Effect of feed supplementation with biosynthesized silver nanoparticles using leaf extract of *Morus indica* L. V1 on *Bombyx mori* L (Lepidoptera: Bombycidae). Scientific Reports 2019;9(1):14839. https://doi.org/10.1038/s41598-019-50906-6. PMid: 31619703.
[67] Sudarsan S, Kumar Shankar M, Kumar Belagal Motatis A, et al. Green synthesis of silver nanoparticles by *Cytobacillus firmus* isolated from the stem bark of *Terminalia arjuna* and their antimicrobial activity. Biomolecules 2021;11(2):259. https://doi.org/10.3390/biom11020259. PMid: 33578957.
[68] Mane PC, Sayyed SA, Kadam DD, et al. Terrestrial snail-mucus mediated green synthesis of silver nanoparticles and *in vitro* investigations on their antimicrobial and anticancer activities. Sci Rep 2021;11(1):13068. https://doi.org/10.1038/s41598-021-92478-4. PMid: 34158586.
[69] Oves M, Rauf MA, Aslam M, et al. Green synthesis of silver nanoparticles by *Conocarpus lancifolius* plant extract and their antimicrobial and anticancer activities. Saudi J Biol Sci 2022;29(1):460–71. https://doi.org/10.1016/j.sjbs.2021.09.007. PMid: 35002442.
[70] Mehata MS. Green route synthesis of silver nanoparticles using plants/ginger extracts with enhanced surface plasmon resonance and degradation of textile dye. Mater Sci Eng B 2021;273:115418. https://doi.org/10.1016/j.mseb.2021.115418.
[71] El-Bendary MA, Moharam ME, Hamed SR, et al. Mycosynthesis of silver nanoparticles using *Aspergillus caespitosus*: Characterization, antimicrobial activities, cytotoxicity, and their performance as an antimicrobial agent for textile materials. Appl Organomet Chem 2021;35(9):e6338. https://doi.org/10.1002/aoc.6338.
[72] Elshafei AM, Othman AM, Elsayed MA, et al. Green synthesis of silver nanoparticles using *Aspergillus oryzae* NRRL447 exogenous proteins: Optimization via central composite design, characterization and biological applications. Environ Nanotechnol Monit Manage 2021;16:100553. https://doi.org/10.1016/j.enmm.2021.100553.
[73] Khan AA, Alanazi AM, Alsaif N, et al. Potential cytotoxicity of silver nanoparticles: Stimulation of autophagy and mitochondrial dysfunction in cardiac cells. Saudi J Biol Sci 2021;28(5):2762–71. https://doi.org/10.1016/j.sjbs.2021.03.021. PMid: 34025162.
[74] Mujaddidi N, Nisa S, Al Ayoubi S, et al. Pharmacological properties of biogenically synthesized silver nanoparticles using endophyte *Bacillus cereus* extract of *Berberis lyceum* against oxidative stress and pathogenic multidrug-resistant bacteria. Saudi J Biol Sci 2021;28(11):6432–40. https://doi.org/10.1016/j.sjbs.2021.07.009. PMid: 34764760.
[75] Barabadi H, Mojab F, Vahidi H, et al. Green synthesis, characterization, antibacterial and biofilm inhibitory activity of silver nanoparticles compared to commercial silver nanoparticles. Inorg Chem Commun 2021;129:108647. https://doi.org/10.1016/j.inoche.2021.108647.
[76] Alharbi NS, Alsubhi NS. Green synthesis and anticancer activity of silver nanoparticles prepared using fruit extract of *Azadirachta indica*. J Radiat Res Appl Sci 2022;15(3):335–45. https://doi.org/10.1016/j.jrras.2022.08.009.
[77] Saravanan A, Kumar PS, Karishma S, et al. A review on biosynthesis of metal nanoparticles and its environmental applications. Chemosphere 2021;264(Part 2):128580. https://doi.org/10.1016/j.chemosphere.2020.128580. PMid: 33059285.
[78] Al-Khattaf FS. Gold and silver nanoparticles: Green synthesis, microbes, mechanism, factors, plant disease management and environmental risks. Saudi J Biol Sci 2021;28(6):3624–31. https://doi.org/10.1016/j.sjbs.2021.03.078. PMid: 34121906.
[79] Hermosilla E, Díaz M, Vera J, et al. Molecular weight identification of compounds involved in the fungal synthesis of AgNPs: Effect on antimicrobial and photocatalytic activity. Antibiotics 2022;11(5):622. https://doi.org/10.3390/antibiotics11050622. PMid: 35625266.
[80] Hashem AH, Saied E, Amin BH, et al. Antifungal activity of biosynthesized silver nanoparticles (AgNPs) against *Aspergilli* causing aspergillosis: Ultrastructure Study. J Funct Biomater 2022;13(4):242. https://doi.org/10.3390/jfb13040242. PMid: 36412883.

[81] Bruna T, Maldonado-Bravo F, Jara P, et al. Silver nanoparticles and their antibacterial applications. Int J Mol Sci 2021;22(13):7202. https://doi.org/10.3390/ijms22137202. PMid: 34281254.
[82] El-Kattan N, Emam AN, Mansour AS, et al. Curcumin assisted green synthesis of silver and zinc oxide nanostructures and their antibacterial activity against some clinical pathogenic multi-drug resistant bacteria. RSC Adv 2022;12 (28):18022–38. https://doi.org/10.1039/d2ra00231k. PMid: 35874032.
[83] Seekonda S, Rani R. Eco-friendly synthesis, characterization, catalytic, antibacterial, antidiabetic, and antioxidant activities of *Embelia robusta* seeds extract stabilized AgNPs. J Sci: Adv Mater Devices 2022;7(4):100480. https://doi.org/10.1016/j.jsamd.2022.100480.
[84] Jyoti K, Baunthiyal M, Singh A. Characterization of silver nanoparticles synthesized using *Urtica dioica* Linn. leaves and their synergistic effects with antibiotics. J Radiat Res Appl Sci 2016;9(3):217–27. https://doi.org/10.1016/j.jrras.2015.10.002.
[85] Khanal LN, Sharma KR, Paudyal H, et al. Green synthesis of silver nanoparticles from root extracts of *Rubus ellipticus* Sm. and comparison of antioxidant and antibacterial activity. J Nanomater 2022;2022(1–11). https://doi.org/10.1155/2022/1832587.
[86] Khan AA, Alanazi AM, Alsaif N, et al. Pomegranate peel induced biogenic synthesis of silver nanoparticles and their multifaceted potential against intracellular pathogen and cancer. Saudi J Biol Sci 2021;28(8):4191–200. https://doi.org/10.1016/j.sjbs.2021.06.022. PMid: 34354399.
[87] Kabir SR, Islam F, Al-Bari MAA, et al. *Asparagus racemosus* mediated silver chloride nanoparticles induce apoptosis in glioblastoma stem cells *in vitro* and inhibit Ehrlich ascites carcinoma cells growth *in vivo*. Arab J Chem 2022;15 (8):104013. https://doi.org/10.1016/j.arabjc.2022.104013.
[88] Alharbi NS, Alsubhi NS, Felimban AI. Green synthesis of silver nanoparticles using medicinal plants: Characterization and application. J Radiation Res Appl Sci 2022;15(3):109–24. https://doi.org/10.1016/j.jrras.2022.06.012.
[89] Kong Y, Paray BA, Al-Sadoon MK, et al. Novel green synthesis, chemical characterization, toxicity, colorectal carcinoma, antioxidant, anti-diabetic, and anticholinergic properties of silver nanoparticles: A chemopharmacological study. Arab J Chem 2021;14(6):103193. https://doi.org/10.1016/j.arabjc.2021.103193.
[90] Moghaddam-Dorafshani M, Jalali M, Nikravesh MR, et al. Study of the effect of hypothyroidism on the apoptotic index in rat ovarian follicles, using the TUNEL technique. Anatom Sci J 2013;10(1):25–36.
[91] Xiao F, Chen D, Luo L, et al. Time-order effects of vitamin C on hexavalent chromium-induced mitochondrial damage and DNA-protein crosslinks in cultured rat peripheral blood lymphocytes. Mol Med Rep 2013;8(1):53–60. https://doi.org/10.3892/mmr.2013.1462. PMid: 23657841.
[92] Dunn D, Turner C. Hypothyroidism in women. Nurs Womens Health 2016;20 (1):93–8. https://doi.org/10.1016/j.nwh.2015.12.002. PMid: 26902444.
[93] Hassanin KM, El-Kawi SHA, Hashem KS. The prospective protective effect of selenium nanoparticles against chromium-induced oxidative and cellular damage in rat thyroid. Int J Nanomed 2013;8(1):1713–20. https://doi.org/10.2147/IJN.S42736. PMid: 23658489.
[94] Mahmood T, Zia Qureshi I, Javed IM. Histopathological and biochemical changes in rat thyroid following acute exposure to hexavalent chromium. Histol Histopathol 2010;25:1355–70. https://doi.org/10.14670/HH-25.1355.
[95] Kalishwaralal K, BarathManiKanth S, Pandian SRK, et al. Silver nanoparticles impede the biofilm formation by *Pseudomonas aeruginosa* and *Staphylococcus epidermidis*. Colloids Surf B Biointerfaces 2010;79(2):340–4. https://doi.org/10.1016/j.colsurfb.2010.04.014. PMid: 20493674.